Supp. Figure 1

a

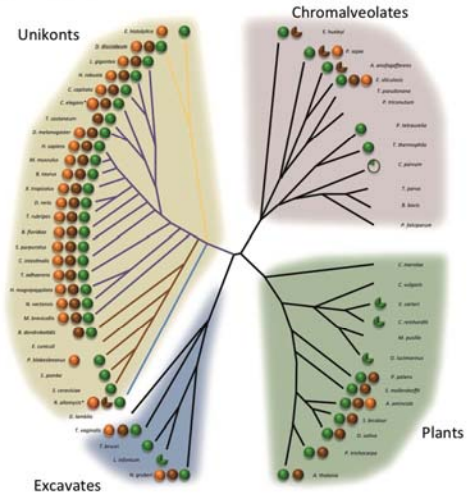

b

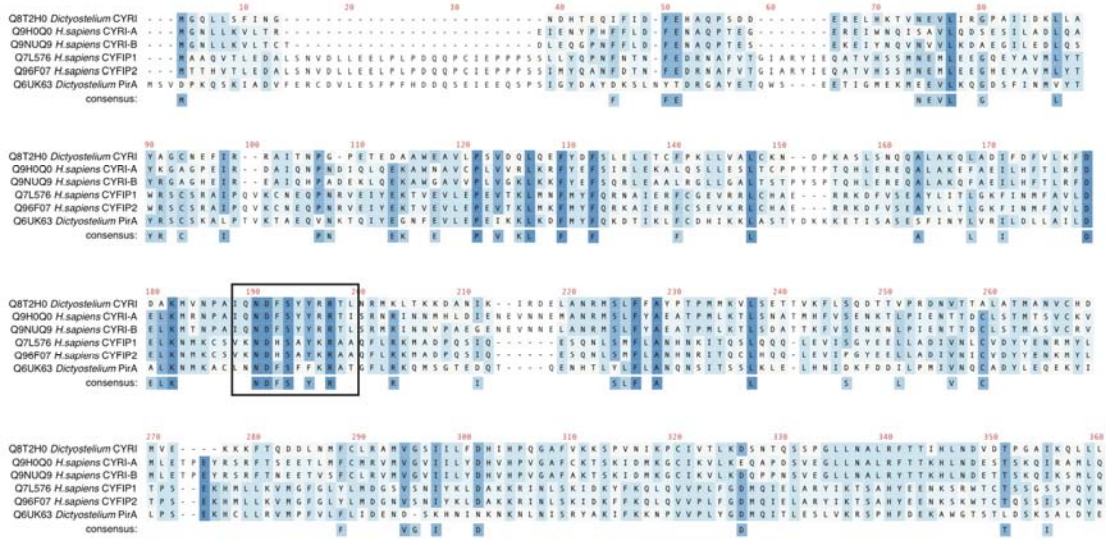

c

Supplementary Figure 1:

CYRI proteins are evolutionarily conserved and contain a putative Rac1 binding site similar to CYFIP.

a - Co-evolution of Arp2/3 (green), Scar/WAVE (brown) and CYRI (orange) across the 4 main superfamilies of the eukaryotic tree 1. An incomplete circle corresponds to the absence of some subunits from the complex as in 2. Each supergroup was assigned to a specific background color: Unikonts (yellow), Chromalveolates (pink), Excavates (blue) and Plants (green). Branch length does not reflect evolutionary distances. For C. elegans and R. allomycis, * and red highlight around circle denotes lack of putative N-terminal myristoylation site on CYRI (see below). Different coloured branches in Unikonts represent amoebazoa (yellow branches), metazoan (purple branches), fungi (brown branches) and Rozella allomycis, the earliest diverged of the fungi (blue branch).

b - Alignment of Dictyostelium discoideum and Homo sapiens CYFIP and CYRI sequences. UniProt accession numbers are reported. Color code represents the number of entries with identical amino acid at this position.

c - HMM logo from the highlighted region in (b). Logo was generated by feeding the full Pfam dataset (915 sequences) of the DUF1394 domain to Skylign. Letter stack represents the conservation of the residue at this position across the dataset. Occupancy score is also mentioned below each letter (light blue) and is a readout of the presence of a letter across the dataset, ranging from 0 (no present) to 1 (present).

Supp. Figure 2

a

Library	CYRI-B interacting domain (aa)	Confidence score (PBS)	Number of fragments
Human Bone Marrow Endothelial Cells	2-324	D	3
Human Breast Tumor Epithelial cells	7-210	D	1
Human Fetal Brain	37-246	D	1
Human Embryonic Stem Cells	39-223	B	5
Human Testis	21-206	D	1
Human Reconstituted Skin	39-324	D	2
Human Leucocytes and Activated Mononuclear cells	9-324	D	2
Human Fibroblasts	20-204	B	13
Human Ventricle and Embryo Heart	19-217	D	7
Human Normal Lung	39-224	D	1
Human Thymocytes	34-210	B	3
Mouse Adult Brain	35-223	D	1

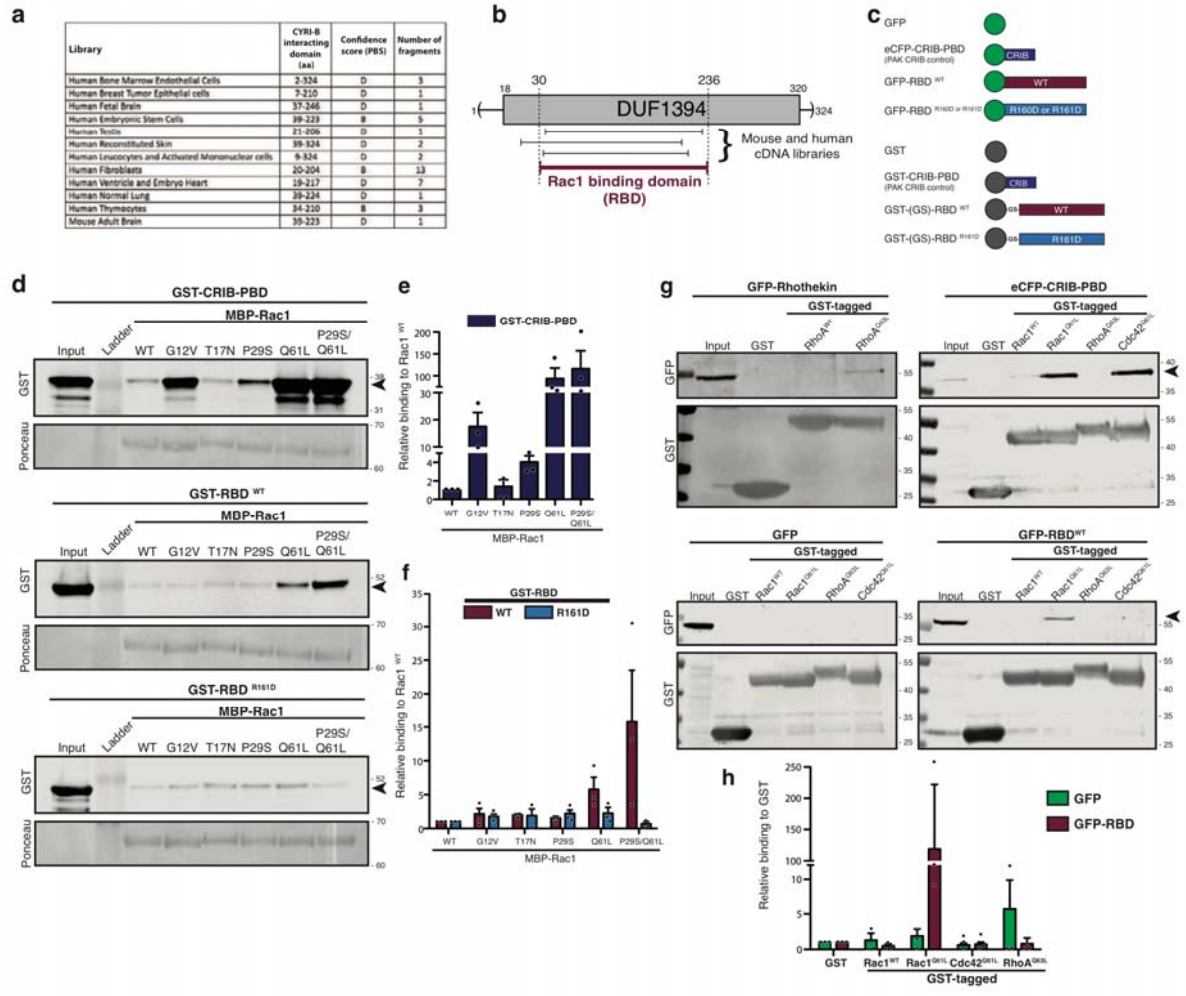

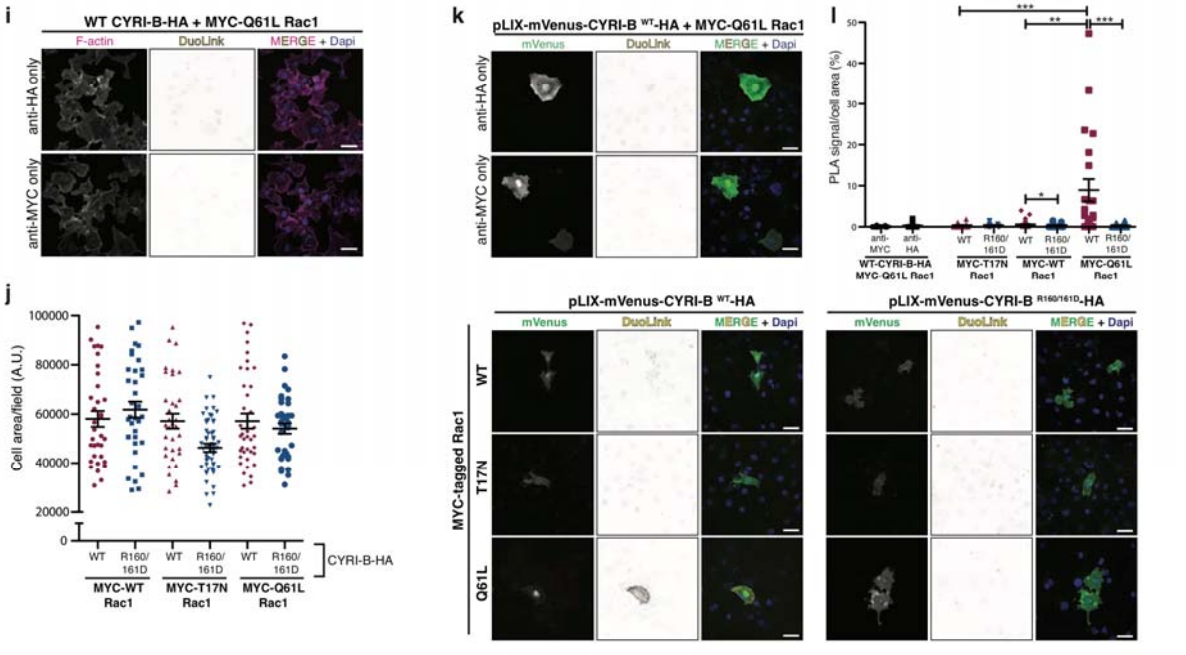

Supplementary Figure 2

CYRI-B interacts directly with active Rac1 *in vitro* and in cells

a - Table presenting the interacting regions between CYRI-B and constitutively active Rac1G12V obtained by a yeast-two hybrid screen. Number of interacting CYRI-B fragments is shown as well as the mapping of this region in the designated library. Confidence score is explained in methods (A=best to D=low).

b - Schematic representation of clones obtained by yeast two-hybrid screening (a) from various mouse and human cDNA libraries. High-confidence interacting regions were used to define a core Rac1-binding domain (RBD) of CYRI-B, stretching from 30-236 amino acids.

c - Schematic representation of various GFP and GST constructs used in pulldown experiments. RBD represents CYRI-B Rac1-binding domain. A Gly-Ser (GS) linker was introduced between GST and CYRI-B RBD for expression purposes. eCFP-CRIB-PBD represents the CRIB region of PAK1, used as a positive control.

d-f – MBP trap beads were loaded with recombinant wild-type (WT) or mutant maltose binding protein MBP-Rac1 protein and incubated with recombinant GST-CRIB-PBD, GST-CYRI-B RBDWT and GST-CYRI-B RBDR161D. Beads were eluted and prepared for western blot analysis. Membrane was blotted for GST. Ponceau staining shows the MBP-Rac1 bands (d). Binding (arrowhead) was analysed by densitometry of each individual band over the input intensity relative to Rac1WT (e-f). (n=3 independent pull down). See also Supplementary Fig. 7.

g-h - GST-pulldowns showing specific binding of CYRI-B RBD to Rac1 over the other Rho GTPases. Lysate from CHL-1 cells expressing GFP (negative control), eCFP-CRIB-PBD, GFP-Rhotekin (reporter for Rac1 or RhoA activity respectively) or GFP-RBDWT were mixed with immbolized GST, GST-Rac1WT, GST-Rac1Q61L, GST-RhoAQ63L, GST-Cdc42Q61L. Membrane was blotted for GFP and GST (g). Binding (arrowhead) was analysed by densitometry of each individual band over the input intensity relative to GST (h). (n=3 independent pull down). See also Supplementary Fig. 7.

i - Control PLA reaction of COS-7 cells co-expressing CYRI-BWT -HA and MYC-Rac1Q61L and incubated with either anti-HA or anti-MYC antibodies and both rabbit and mouse PLA probes. PLA signal (yellow), F-actin (magenta) and nuclei (blue). Scale bar = 50 µm.

j - Cell area was measured for each field of view (fov) and plotted. Average cell area was similar between conditions. (Myc-WT/WT-HA n=34 fov; Myc-WT/R160-161D-HA n=35 fov; Myc-T17N/WT-HA n=34 fov; Myc-T17N/ R160-161D-HA n=55 fov; Myc-Q61L/WT-HA n=39 fov; Myc-Q61L/ R160-161D-HA n=36 fov)

k-l - Proximity ligation assay was performed on COS-7 cells plated on laminin and co-expressing pLIX-mVenus-CYRI-B-HA (wild-type or mutant R160/161D) and different MYC-tagged Rac1 constructs.

Cells were first incubated with a mouse anti-HA-tag and a rabbit ant-MYC-tag antibody, followed by both PLA probes. PLA signal (yellow), mVenus transfection reporter (green) and nuclei (blue). Negative controls were performed on cells co-expressing CYRI-BWT-HA and MYC-Rac1Q61L and incubated with either antibody (anti-HA only or anti-MYC only) and both rabbit and mouse PLA probes (k). Randomised fields of view were acquired across 2 independent experiments. PLA signal was quantified by a thresholding method using Fiji and reported to the cell area using the GFP signal (l).

One-way ANOVA with Dunn's post-test was performed between CYRI-BWT and the different MYC-Rac1 constructs. Two-tailed Mann Whitney test was tested between CYRI-BWT and CYRI-BR160/161D for each MYC-Rac1 construct. * $p \leq 0.05$, ** $p \leq 0.01$, *** $p \leq 0.001$. (anti-HA n=34 ; anti-Myc n=33 ; Myc-WT/WT-HA n=40 ; Myc-WT/R160/161D-HA n=30 ; Myc-T17N/WT-HA n=63 ; Myc-T17N/ R160/161D-HA n=34 ; Myc-Q61L/WT-HA n=22 ; Myc-Q61L/R160/161D-HA n=40)

Scale bar = 50 µm.

All data presented are representative of at least 3 biologically independent experiments except if stated otherwise.

Bar and scatter plots show data points with mean and S.E.M.

Supp. Figure 3

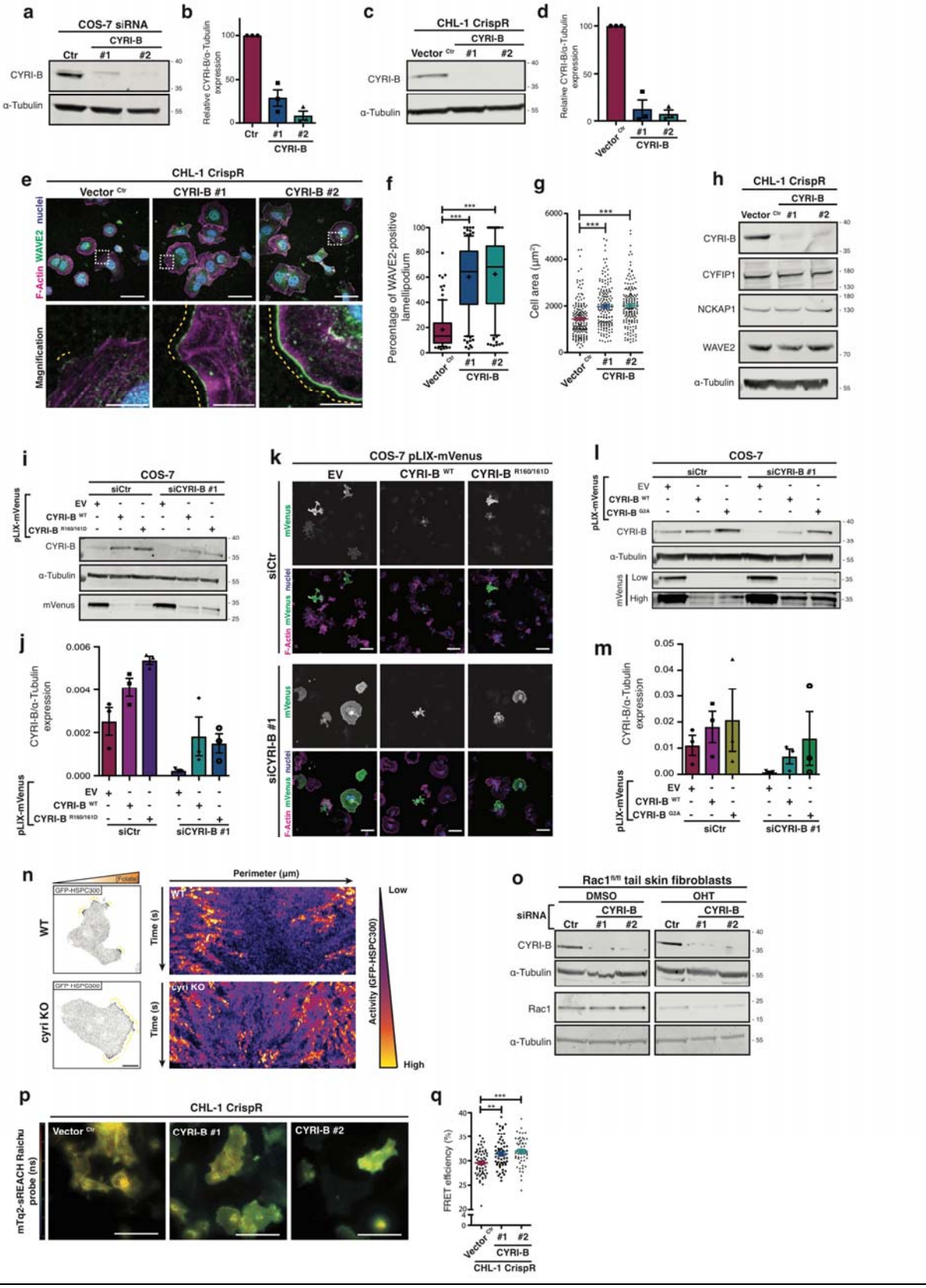

Supplementary Figure 3

CYRI proteins oppose Rac1-dependent recruitment of Scar/WAVE complex to the leading edge

a-b - Western blot of CYRI-B and α-Tubulin expression after CYRI-B knockdown by siRNA in COS-7 cells. (a). Quantification by densitometry normalised to the control Scramble siRNA (b). (n=3 independent western blot)

c-d - Establishment of 2 independent cyri-b knockout CHL-1 cell lines using CrispR-Cas9 was confirmed by western blot using 2 independent guide RNA (sequences #1 and #2). Membrane was blotted for CYRI-B and α-Tubulin (c). CYRI-B expression was quantified after puromycin selection and normalised to the control (Vector Ctr) CrispR cell line (d). (n=3 independent western blot)

e-g - Immunofluorescence of control (Vector Ctr) or each of two independent cyri-b knockout CHL-1 cell lines (#1 and #2) plated on collagen-I for 4 hours and stained for WAVE2 (green), nuclei (blue) and F-actin (magenta). Scale bar = 50 μm. Box insets show a magnified field of the designated area below each panel. Scale bar = 10 μm. (e).

The ratio of extension of WAVE2 staining (yellow dotted line) vs the total cell perimeter shown in (f) is a read-out of the extent of the cell edge devoted to lamellipodium. Manual quantification of cell area (g) is shown. One-way ANOVA with Dunn's post-test was performed. *** $p \leq 0.001$. (e-f: Ctr n=89 cells, #1 n=109 cells, #2 n=97 cells – g: Ctr n=286 cells, #1 n=257 cells, #2 n=245 cells).

h - Western blot analysis of control (Vector Ctr) or cyri-b CrispR knockout CHL-1 cell lines (#1 and #2), probed for Scar/WAVE complex members and α-Tubulin.

i-k - Western blot confirming the re-expression of siRNA-resistant construct. Scramble or siCYRI-B-treated COS-7 cells were transfected with doxycycline-inducible pLIX-mVenus empty vector (EV) or containing a siRNA-resistant CYRI-B sequence (WT or R160/161D). Cells were induced for 48h and lysed for western blot against CYRI-B, α-Tubulin or GFP (cross-react with mVenus) (i). Rescue was confirmed by densitometry as shown in (j) (n=3 independent western blot). Representative pictures (k) of the rescue experiment quantified in Figure 3 e-f. Scale bar = 50 μm

l-m - Western blot confirming the re-expression of siRNA-resistant construct. Scramble or siCYRI-B-treated COS-7 cells were transfected with doxycycline-inducible pLIX-mVenus empty vector (EV) or containing a siRNA-resistant CYRI-B sequence (WT or G2A). Cells were induced for 48h and lysed for western blot analysis. Membrane was blotted for CYRI-B, α-Tubulin or GFP (cross-react with mVenus). Given the low expression level of some constructs, two exposures of the same blot for GFP is shown (l). Rescue was confirmed by densitometry as shown in (m) (n=3 independent western blot).

n - Still picture from a timelapse movie presenting WT and cyri KO Ax3 cells, transfected with GFP-HSPC300 and migrating in a squashed under agarose chemotaxis assay. Yellow dotted lines highlight the length of GFP-HSCP300 accumulation along the cell edge. Scale bar = 5 μm. See also Supplementary Movie 1. Polar kymograph presenting the Scar/WAVE complex activity at the cell cortex.

o - Western blot analysis of ROSA26::Cre-ERT2+;p16Ink4a-/-; Rac1fl/fl mouse tail fibroblasts treated 7 days with DMSO or OHT to induce Rac1 recombination. Cells were further transfected with Scramble (Ctr) or mouse specific Cyri-B siRNA (#1 and #2). Membrane was blotted for CYRI-B, Rac1 and α-Tubulin.

p-q - FLIM/FRET experiment realised on control (Vector Ctr) or cyri-b knockout (#1 and #2) CHL-1 cells transfected with the Raichu-Rac1 probe and plated on collagen. The jet2 color code shows the average lifetime of the probe, spanning 1-4 ns (blue to red) (p). Quantification of the FRET efficiency obtained in CHL-1 cells is plotted in (q). One-way ANOVA with Dunn's post-test was performed. ** $p \leq 0.01$, *** $p \leq 0.001$. (Ctr n=61 cells, #1 n=63 cells, #2 n=56 cells).

Scale bar = 50 μm. (n=3 independent assays)

All data presented are representative of at least 3 biologically independent experiments. For a, c, h, l, l and o see also Supplementary Fig. 7.

Bar and scatter plots show data points with mean and S.E.M.

Whisker plots show 10-90 percentile, median (bar) and mean (cross).

Supp. Figure 4

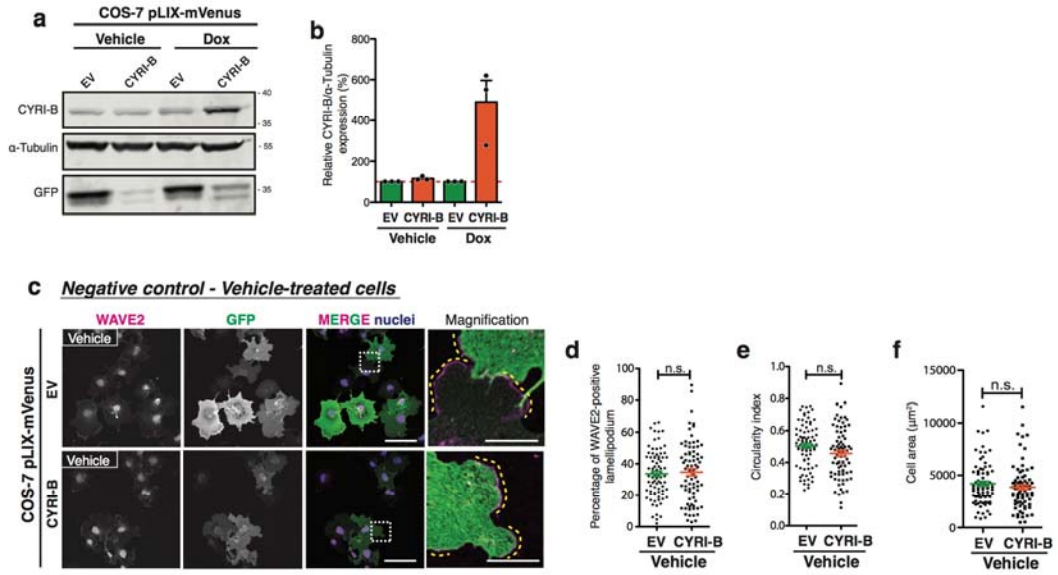

Supplementary Figure 4

Cells containing CYRI-B inducible vector but treated with the vehicle solution show similar phenotype to the control cells

a-b - Western blot of COS-7 cells transiently transfected with a mVenus-TetON inducible CYRI-B construct probed with anti-GFP (detects mVenus co-expression). Cells were collected and analysed 48h after vehicle or doxycycline treatment (a). Percentage of overexpression relative to the EV (standardised at 100% - Red dotted line) (b) (n=3 independent western blot). See also Supplementary Fig. 7.

c-f - Immunofluorescence of vehicle-treated negative control (EV) or CYRI-B COS-7 cells, fixed after 4h of spreading and stained for WAVE2 (magenta), nuclei (blue) and GFP (green). Scale bar = 50 µm. Inset panels are a magnified view of the white dashed field. Scale bar = 10 µm (c). WAVE2 ratio and circularity were measured and reported in (d) and (e) respectively. Cell area quantification was based on the phalloidin staining (f). Two-tailed Mann-Whitney test was applied. n.s. $p > 0.05$. (Veh/EV n=81 cells ; Veh/CYRI-B n=78 cells).

All data presented are representative of at least 3 biologically independent experiments.

Bar and scatter plots show data points with mean and S.E.M.

Supp. Figure 5

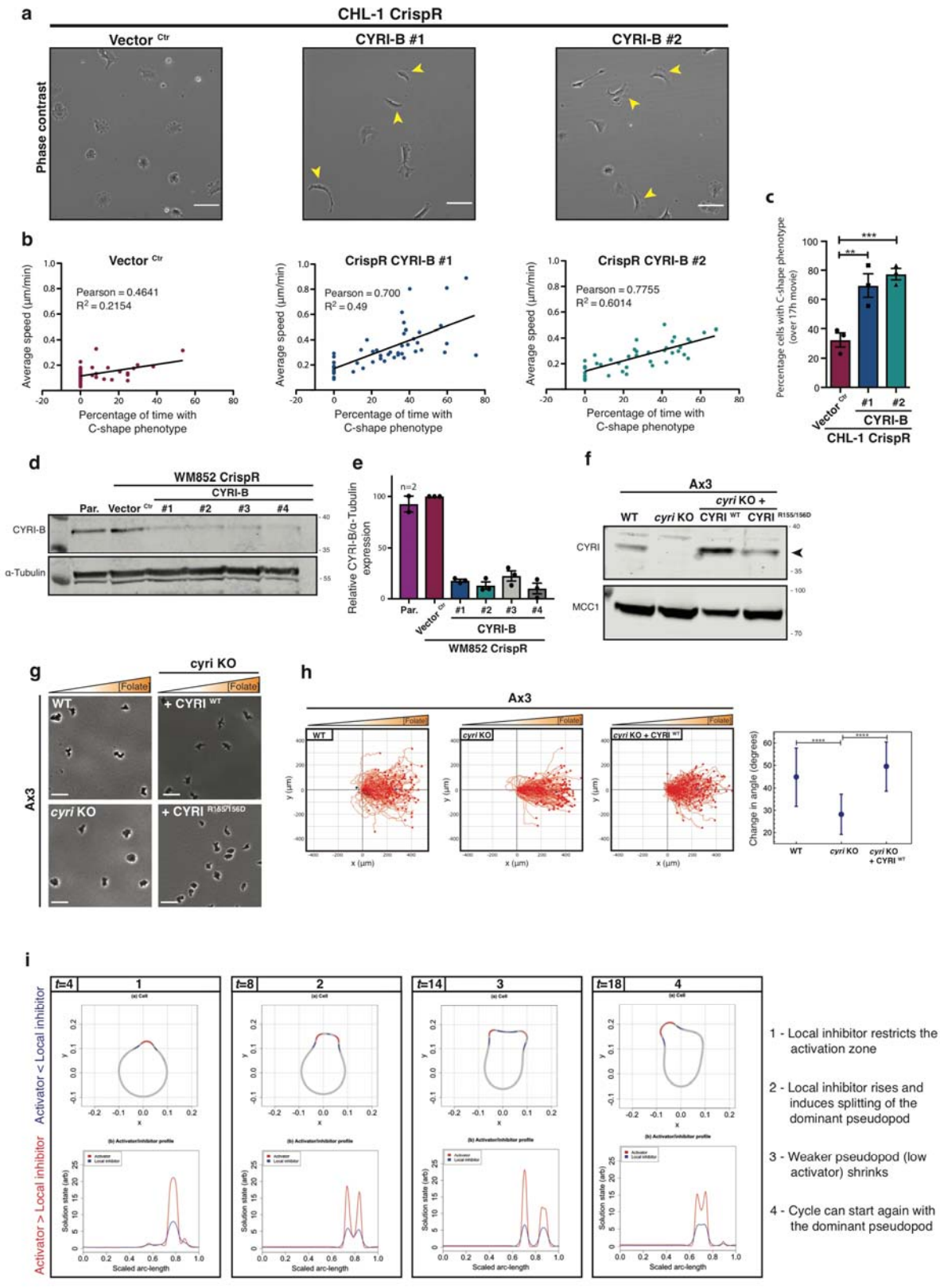

Supplementary Figure 5

CYRI regulates cell shape and motility and acts as a Meinhardt local inhibitor

a - Still phase contrast pictures from a random migration assay of control (Vector Ctr) or cyri-b CrispR knockout (#1 and #2) CHL-1 cells plated on collagen-I-coated glass bottom dishes. Yellow arrowheads denote C-shaped cells. Scale bar = 100 µm (Movie S4).

b - Correlation between cell shape and average speed in control (Vector Ctr) or cyri-b CrispR knockout (#1 and #2) CHL-1 cells. Pearson coefficient and R2 value are shown for each condition. (Ctr n=45 cells, #1 n=53 cells, #2 n=42 cells)

c - Random migration assay movies were analysed and the percentage of cells presenting a C-shape during the time of the experiment is reported. Cochran-Mantel-Haenszel test was performed. ** p≤0.001; *** p≤0.0005. (n=3 independent assay representing >75 cells)

d-e - Western blot analysis of CYRI-B expression in parental (Par.), CrispR control (Vector Ctr) or four independent cyri-b CrispR knockout WM852 melanoma cells (CYRI-B #1-4). Membrane was blotted for CYRI-B and α-Tubulin (d). Bar graph (e) represents quantification of CYRI-B expression relative to the Vector Ctr cell line. (n=3 independent western blot except for Parental cell line n=2, see also Supplmentary Fig. 7).

f - Establishment of cyri knockout and CYRI rescued Ax3 D. discoideum cells was confirmed by western blot analysis. Membrane was blotted for D. discoideum CYRI (arrowhead) and MCC1 as a loading control. See also Supplementary Fig. 7.

g - Representative phase contrast pictures from an under agarose chemotaxis assay of Ax3 (WT) and Ax3-derived cell lines migrating towards a folate gradient, as illustrated (Movie S7). Scale bar = 25 µm

h - Cells chemotaxing in a folate under-agarose experiment were tracked automatically using an ImageJ plugin (see material and methods). To monitor the persistence of cell movement, the angle between each step was calculated from x and y positions at each time point and is plotted on the right-hand side graph (Mean and S.D. are shown). One-way ANOVA with Dunn's post-test was performed. **** p≤0.0001. (WT n=424 cells, cyri KO n=581 cells, cyri KO + CYRIWT=727 cells).

i - Pictures extracted from the modelling of CYRI proteins as local inhibitor (Supp. movie S9). In each panel, top graph shows the outline of a simulated cell, with red areas of the periphery having more activator than local inhibitor and blue having more local inhibitor than activator. The x- and y-axes correspond to arbitrary units representing distance. The simulation was run from time t=0 and panels are taken from times shown (arbitrary units of time). Bottom graph shows the concentrations of the activator (red) and the local inhibitor (blue), where the x-axis represents the scaled arc-length around the perimeter of the cell and the y-axis represents the concentration in arbitrary units. Panel 1 (t=4) shows the generation of a pseudopod, where the local inhibitor causes the edges of the activated region to sharpen. Panel 2 (t=8) shows a split in the activator profile (and, consequently, a split in the associated pseudopod), which results from the higher relative concentration of the local inhibitor near the centre of the activated region. Panel 3 (t=14) shows the cell with two smaller pseudopods, which compete for dominance and determine the direction of migration. Panel 4 (t=18) shows the winning pseudopod starting the cycle over again and the local inhibitor rising in response to the rise in activator.

All data presented are representative of at least 3 biologically independent experiments except if mentioned otherwise.

Bar and scatter plots show data points with mean and S.E.M.

Supp. Figure 6

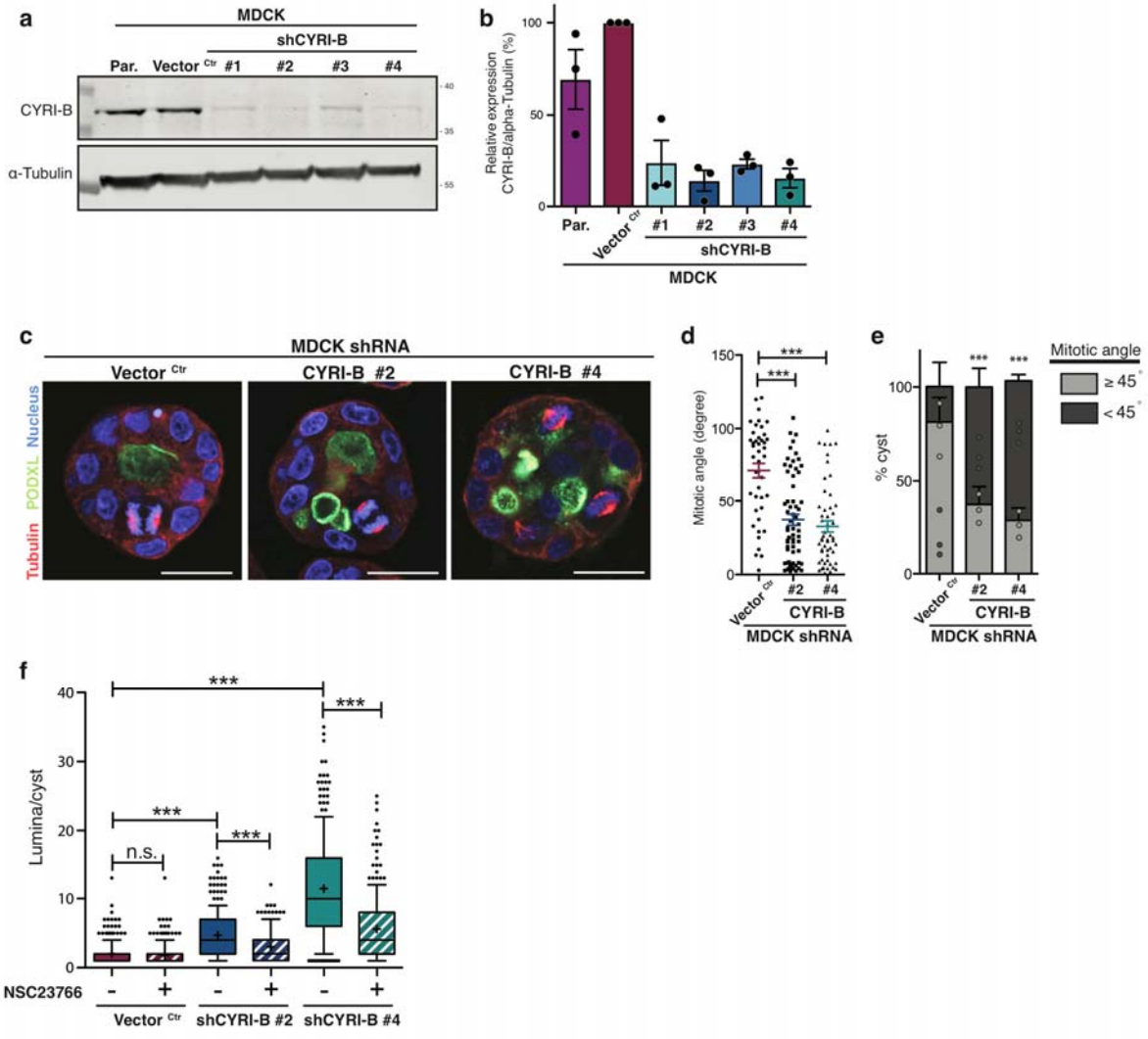

Supplementary Figure 6

CYRI-B regulates mitotic angle and Rac1-dependent lumenogenesis

a-b - Western blot analysis of parental (Par.), shRNA Control (Vector Ctr) or four independent shCYRI-B MDCK cell lines. Membranes were blotted against CYRI-B and α-Tubulin (a). Bar graph represents quantification of CYRI-B expression relative to the control cell line (b) (n=3 independent western blot). See also Supplementary Fig. 7.

c-e - Immunofluorescence of control (Vector Ctr) or cyri-b knockdown MDCK cysts grown in 3D. Cysts were fixed after 5 days and stained for Pdx1 (green), Tubulin (red) and nuclei (blue). Scale bar = 25 μm (c). Mitotic angle (formed between mitotic spindle axis and apico-basal axis) was quantified in (d). One-way ANOVA with Dunn's post-test was performed. *** $p \leq 0.001$. Angles were divided as greater (normal) or lower (abnormal) than 45 degrees and plotted as a bar graph (e). Two-tailed Chi-square test (95% confidence) was applied for each condition compared with the control cells. *** $p \leq 0.001$. (d-e: Ctr n=43 cysts, #1 n=64 cysts, #2 n=53 cysts)

f - Number of lumina from control (Vector Ctr) or cyri-b knockdown cysts treated or not with 100 μM NSC23766. One-Way ANOVA with Dunn's post-test was applied between vehicle-treated knockdown cysts and vehicle-treated control cysts. Unpaired two-tailed t-test was applied to untreated versus treated cysts. n.s. $p>0.05$, *** $p \leq 0.001$. (Ctr/Veh n=248 cysts ; Ctr/NSC n=248 cysts; #1/Veh n=242 cysts; #1/NSC n=243 cysts; #2/Veh n=243 cysts; #2/NSC n=239 cysts).

All data presented are representative of at least 3 biologically independent experiments.

Bar and scatter plots show data points with mean and S.E.M.

Whisker plots show 10-90 percentile and mean (cross).

Supp. Figure 7

Figure 1

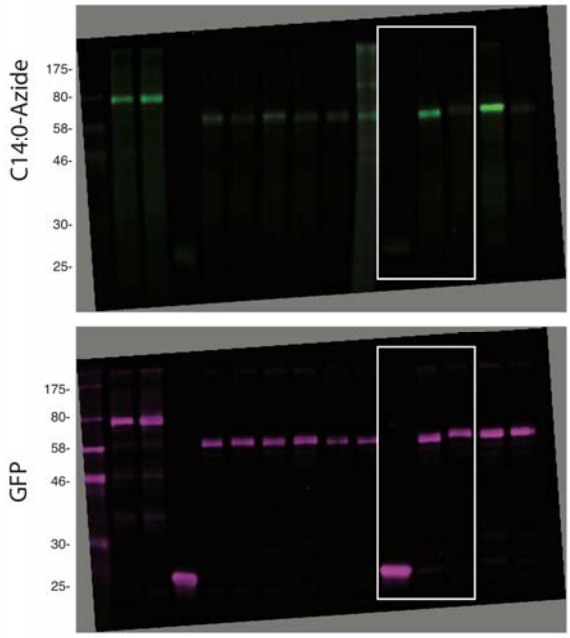

Supplementary Figure 7
Unprocessed western blot
Pictures of individual blots shown throughout this study

Supp. Figure 7

Figure 2

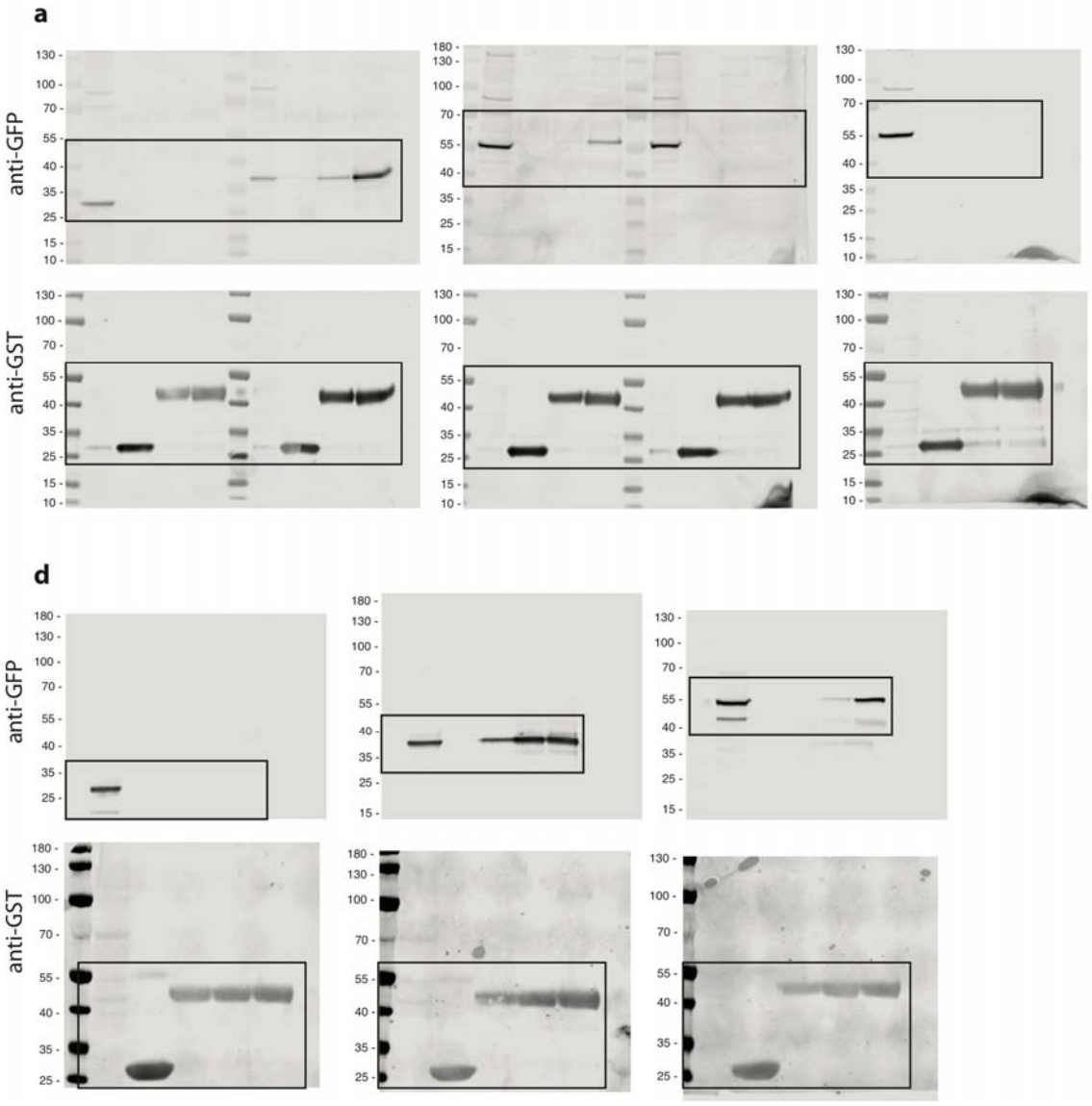

Supplementary Figure 7
Unprocessed western blot
Pictures of individual blots shown throughout this study

Supp. Figure 7 continued

Figure 3

n

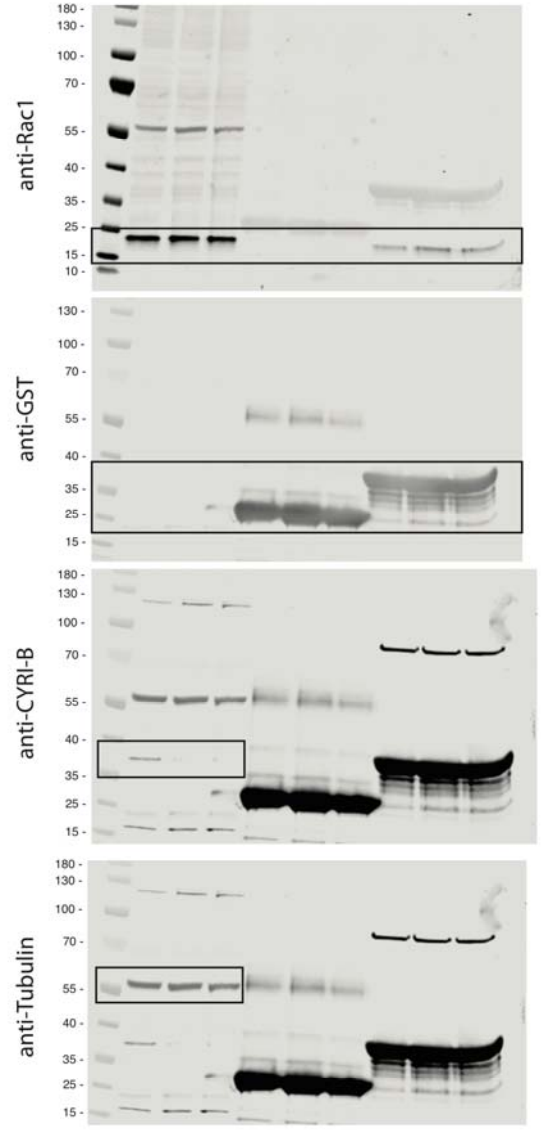

Supplementary Figure 7
Unprocessed western blot
Pictures of individual blot shown throughout this study

Supp. Figure 7 continued

Supp. figure 2

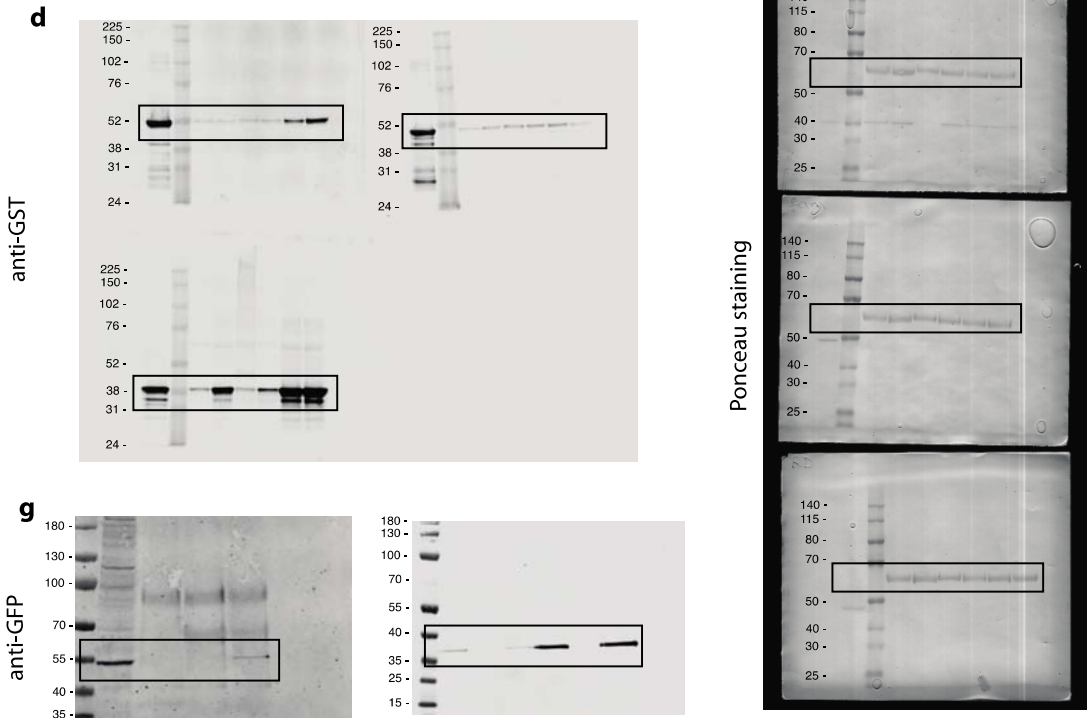

Supplementary Figure 7
Unprocessed western blot
Pictures of individual blots shown throughout this study

Supp. Figure 7 continued

Supp. figure 3

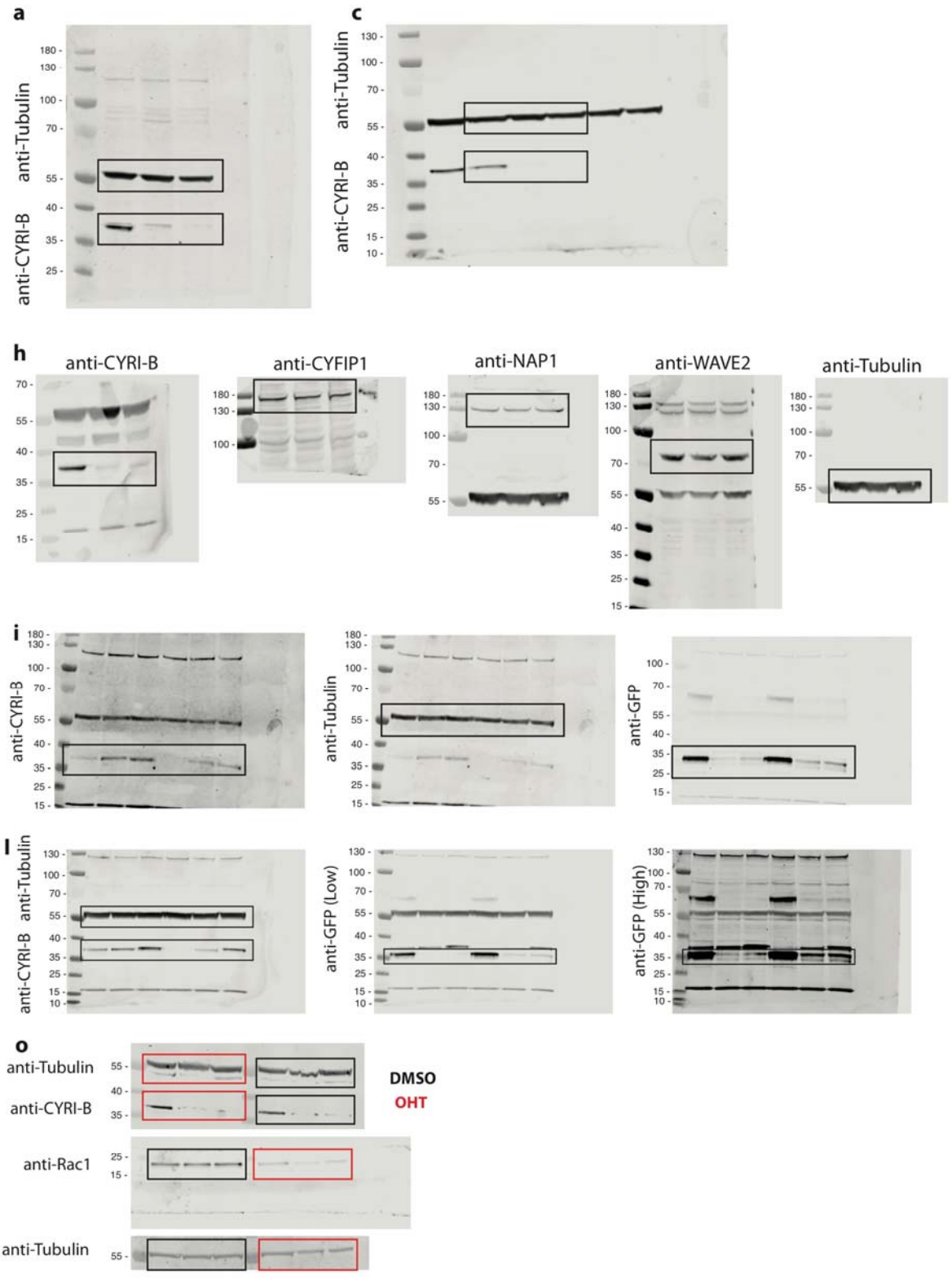

Supplementary Figure 7
Unprocessed western blot
Pictures of individual blots shown throughout this study

Supp. Figure 7 continued

Supp. figure 4

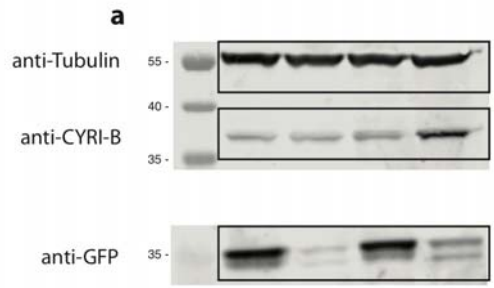

Supplementary Figure 7
Unprocessed western blot
Pictures of individual blots shown throughout this study

Supp. Figure 7 continued

Supp. figure 5

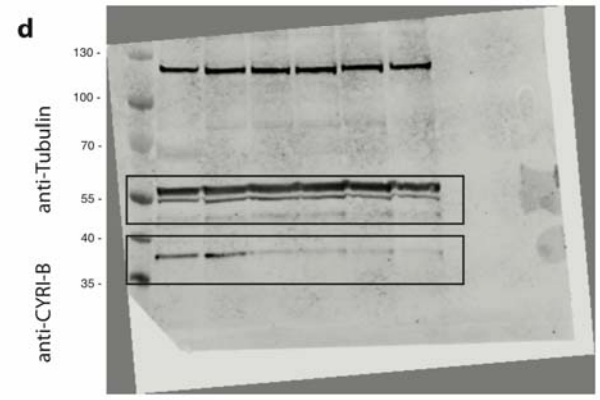

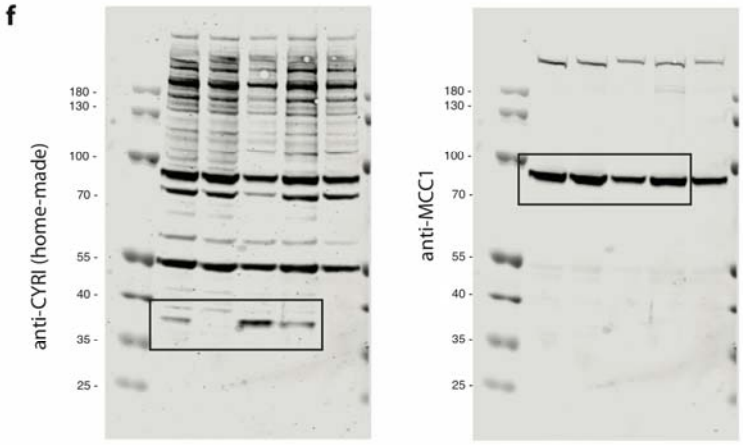

Supplementary Figure 7
Unprocessed western blot
Pictures of individual blots shown throughout this study

Supp. Figure 7 continued

Supp. figure 6

a

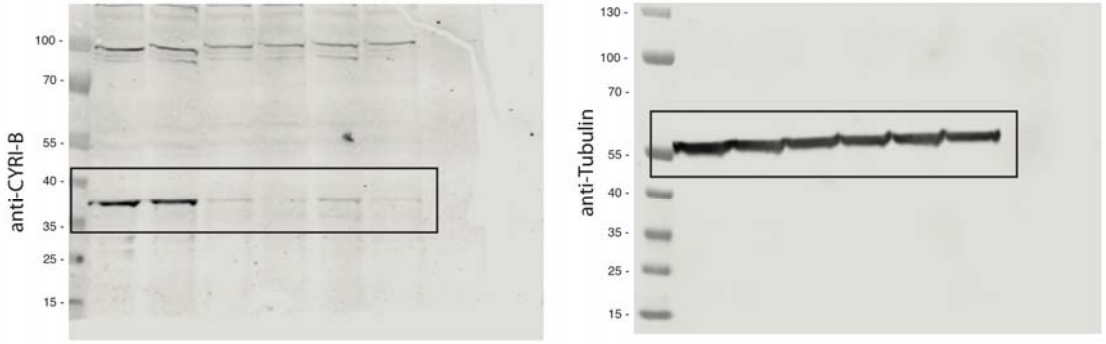

Supplementary Figure 7
Unprocessed western blot
Pictures of individual blot shown throughout this study

Supplementary video 1: *cyri* KO Ax3 cells show a broader recruitment of the Scar/WAVE complex.
Under-agarose chemotaxis assay toward folate of wild type or *cyri* KO Ax3 cells transfected with HSPC300-GFP.
1frame/6sec
Scale bar = 10 μm.
Experiment was repeated independently 3 times with similar results

Supplementary video 2: Automatic segmentation of the cell edge
Segmentation of CrispR control (Vector Ctr) or *cyri-b* knockout (cyri-b #1) CHL-1 cells, transfected with GFP-LifeAct. Cell periphery is shown in magenta.
1 frame/sec.
Scale bar = 25 μm.

Supplementary video 3: *cyri-b* KO MEFs show a defect in the restriction of Rac1-induced protrusions.
Time-lapse movie of control (DMSO - top) and CYRI-B $^{-/-}$ (OHT - bottom) MEF cells, transfected with the photo-activable mCherry Rac1 probe. Phase and mCherry channels are shown as a merge. Probe is locally photo-activated (blue circle area) after 1 min (top left label switches for "DARK" to "458 nm").
1 frame/2 sec.
Scale bar = 25 μm.
Experiment was repeated independently 4 times with similar results.

Supplementary video 4: Loss of CYRI-B promotes a more migratory phenotype in CHL-1 cells.
Random migration assay of control (Vector Ctr) or *cyri-b* CrispR knockout (#1 and #2) CHL-1 cells. Movies are representative of an 8h timelapse experiment.
Scale bar = 100 μm
1 frame/10min
Experiment was repeated independently 3 times with similar results

Supplementary video 5: *cyri-b* KO WM852 cells lose their ability to chemotax toward FBS.
Chemotaxis assay using control (Vector Ctr), or *cyri-b* CrispR knockout (#1 and #2) WM852 cells. Cells are migrating from a serum-free environment (Left side of each movie) to a 10% FBS supplemented media (right side of each movie). Tracks are displayed for this movie.
Scale bar = 50 μm
1 frame/15min
Experiments was repeated independently 4 times with similar results

Supplementary video 6: Expression of CYRI^{WT} but not the Rac1-binding defective mutant rescues the shape phenotype associated with the loss of CYRI in *D. discoideum*
DIC movie from a under agarose chemotaxis assay of WT, *cyri* KO, or the REMI rescue strains (*cyri* KO + CYRI^{WT} and *cyri* KO + CYRI$^{R155/156D}$) migrating toward folate.
1 frame/2sec
Scale bar = 25 μm

Experiment was repeated independently 3 times with similar results

Supplementary video 7: Expression of CYRI^{WT} but not the Rac1-binding defective mutant rescues the migratory phenotype associated with the loss of CYRI in *D. discoideum*
Phase contrast movie from an under agarose chemotaxis assay toward folate.
Scale bar = 100 μm
1frame/30sec
Experiment was repeated independently 3 times with similar results

Supplementary video 8: *cyri* KO Ax3 cells have a defect to reorientate their pseudopod toward a sharp gradient of cAMP
Needle assay using WT or *cyri* knockout Ax3 cells, responding to cAMP.
1 frame/5sec.
Scale bar = 20 μm
Experiment was repeated independently 4 times with similar results

Supplementary video 9: Mathematical model of a cell protrusion and motility.
Cell protrusions are generated following an increase of an activator (Red: Rac1 or Scar/WAVE complex), cross-talking to a local inhibitor (Blue: CYRI) that restricts pseudopod width. Accumulation of the local inhibitor causes pseudopod spitting. See text for more details.

Supplementary Table 1: Gene and protein nomenclature
Gene and protein nomenclature based on HGNC guidelines

Supplementary Table 2: Significant candidates obtained from NAP1 pull down after reversible crosslink treatment in *D. discoideum*
Uniprot accession numbers are listed for each putative interactor. Welch's t test and further analysis were performed using MaxQuant software.

Supplementary Table 3: List of Antibodies
Information regarding provider, catalog number and working dilution of antibodies and fluorescent probes/stains used in this study.

Supplementary Table 4: List of constructs
Information regarding the plasmids used in this study

Supplementary Table 5: List of siRNA, shRNA, gRNA and primers
Sequence corresponding to the oligos used in this study

Supplementary Table 6: Statistics Source Data
Individual data points presented in this study.

Supplementary Note 1 (Plugin 1): Image Analysis for PA-Rac1

To produce overlay images to highlight the protrusive activity, mCherry images were used to compare frames 1 and 30, as the baseline activity, and frames 30 and 150, to show the Rac1-induced protrusive activity. In Fiji, frames 1, 30, and 150 were pulled out, images changed to 8 bit, levels were adjusted to optimize signal for frame 150 due to photobleaching, images converted to binary 255/0 by thresholding, noise removed (a sequence of Analyze Particles >1000 and Despeckle), and the cell outline set at 255. The overlapping cell area that neither protruded or retracted was produced (Image Calculator, frame 30 x 150). The protrusion and retraction areas were produced (Protrusion = frame 150 – overlap; Retraction = frame 30 – overlap), and the cell outline in each case converted to white as 255 with background black as 0 (Invert Image; Invert LUT). Color coded overlay images were produced (Merge Images, overlay assigned grey, protrusion assigned blue, retraction assigned magenta), and then the background converted to white (Paint fill tool). From the overlay images, or the separate protrusion and retraction images, areas were quantified in Fiji. The spread of protrusion was measured in Fiji by drawing lines in the main protrusion area, defined as the protrusion uninterrupted by any retraction areas, from the edge of the protrusion area to the nearest edge of the photoactivation area, on both sides to get an average spread distance.

A Fiji plugin was developed for this step:

Supplementary Note 2 (Plugin 2): Automated tracking plugin for under-agarose chemotaxis assay.
A Fiji plugin was developed to measure in an unbiased and automatic way, *D. discoideum* migrating in an under-agarose assay.

Supp. Plugin 1 - Image Analysis - PA-Rac1 experiment

```
rename("WORKING");
run("Split Channels");
selectWindow("C2-WORKING");
close();

selectWindow("C1-WORKING");
getDimensions(width,height,channels,slices,frames);

run("Duplicate...", "title=MASK duplicate");
run("Convert to Mask", "method=Triangle background=Dark calculate black");
run("Remove Outliers...", "radius=0.5 threshold=50 which=Bright stack");
run("Remove Outliers...", "radius=0.5 threshold=50 which=Dark stack");
//run("Fill Holes", "stack");

run("Analyze Particles...", "size=400-Infinity show=Masks in_situ stack");

setSlice(30);
run("Duplicate...", "title=BEFORE");
selectWindow("MASK");
setSlice(150);
run("Duplicate...", "title=AFTER");
selectWindow("BEFORE");
run("Divide...", "value=3");

selectWindow("C1-WORKING");
selectWindow("AFTER");
run("Calculator Plus", "i1=AFTER i2=BEFORE operation=[Subtract: i2 = (i1-i2) x k1 +
k2] k1=1 k2=0 create");
run("Calculator Plus", "i1=BEFORE i2=AFTER operation=[Subtract: i2 = (i1-i2) x k1 +
k2] k1=1 k2=0 create");
rename("RETRACTED");
run("Calculator Plus", "i1=RETRACTED i2=Result operation=[Add: i2 = (i1+i2) x k1 +
k2] k1=1 k2=0 create");
run("LT GM RacLUT");
rename("BeforeAfterOverlay");

run("Set Measurements...", "area area_fraction redirect=None decimal=3");

selectWindow("RETRACTED");
setThreshold(64, 115);
run("Convert to Mask");

selectWindow("C1-WORKING");
run("Properties...", "channels=1 slices=1 frames="+frames+" unit=micron
pixel_width=0.1317882 pixel_height=0.1317882 voxel_depth=1.0000000
frame=[3.26 sec] global");
selectWindow("RETRACTED");
run("Analyze Particles...", "    show=Nothing summarize");
```

```
selectWindow("Result");
rename("EXTENDED");

setThreshold(250, 255);
run("Convert to Mask");
run("Analyze Particles...", "summarize");

selectWindow("AFTER");
close();
selectWindow("BEFORE");
close();
selectWindow("MASK");
close();
selectWindow("EXTENDED");
close();
selectWindow("RETRACTED");
close();
```

Supp. plugin 2 - Automated tracking plugin for under-agarose chemotaxis assay.

```
run("Convert to Mask", "method=IsoData background=Dark calculate black");
run("Invert", "stack");
run("Analyze Particles...", "size=400-Infinity pixel circularity=0.00-1.00 show=Masks in_situ stack");
run("Fill Holes", "stack");
run("Set Measurements...", "area centroid shape stack redirect=None decimal=3");
run("Analyze Particles...", "size=0-Infinity circularity=0.00-1.00 show=Nothing display clear summarize stack");
```

nature research

Corresponding author(s): Laura M Machesky, Robert H Insall

Reporting Summary

Nature Research wishes to improve the reproducibility of the work that we publish. This form provides structure for consistency and transparency in reporting. For further information on Nature Research policies, see Authors & Referees and the Editorial Policy Checklist.

Statistical parameters

When statistical analyses are reported, confirm that the following items are present in the relevant location (e.g. figure legend, table legend, main text, or Methods section).

n/a	Confirmed
☐	☒ The exact sample size (*n*) for each experimental group/condition, given as a discrete number and unit of measurement
☐	☒ An indication of whether measurements were taken from distinct samples or whether the same sample was measured repeatedly
☐	☒ The statistical test(s) used AND whether they are one- or two-sided *Only common tests should be described solely by name; describe more complex techniques in the Methods section.*
☐	☒ A description of all covariates tested
☐	☒ A description of any assumptions or corrections, such as tests of normality and adjustment for multiple comparisons
☐	☒ A full description of the statistics including central tendency (e.g. means) or other basic estimates (e.g. regression coefficient) AND variation (e.g. standard deviation) or associated estimates of uncertainty (e.g. confidence intervals)
☐	☒ For null hypothesis testing, the test statistic (e.g. *F*, *t*, *r*) with confidence intervals, effect sizes, degrees of freedom and *P* value noted *Give P values as exact values whenever suitable.*
☒	☐ For Bayesian analysis, information on the choice of priors and Markov chain Monte Carlo settings
☒	☐ For hierarchical and complex designs, identification of the appropriate level for tests and full reporting of outcomes
☒	☐ Estimates of effect sizes (e.g. Cohen's *d*, Pearson's *r*), indicating how they were calculated
☐	☒ Clearly defined error bars *State explicitly what error bars represent (e.g. SD, SE, CI)*

Our web collection on statistics for biologists may be useful.

Software and code

Policy information about availability of computer code

Data collection	Image-J (NIH v 1.48t), ImageStudioLite (LICOR Biosciences Ltd v.5.2.5), XCalibur (ThermoFisher Scientific), Metamorph (Molecular Device v.7.8.13), FV10-ASW (Olympus v. 4.2), NIS-ELEMENT AR (Nikon v. 4.5), Zen (Zeiss v.3.2 SP1), LI-FLIM (Lambert Instruments v. 1.2.12), BiaCore T200 evaluation software (GE Healthcare)
Data analysis	Image-J (NIH v 1.48t), ImageStudioLite (LICOR Biosciences Ltd v.5.2.5), MaxQuant (v.1.5.5.1), Scaffold (Proteome Software v 4.3.2), Prism (GraphPad v 5.0c and v 7.0), BiaCore T200 evaluation software (GE Healthcare), Metamorph (Molecular Device v.7.8.13), Zen (Zeiss v.3.2 SP1), LI-FLIM (Lambert Instruments v. 1.2.12), Supplementary Note 1, Supplementary Note 2, Microsoft Excel 2011 (v 14.7.3), Imaris (BitPlane v. 9.1.0).

For manuscripts utilizing custom algorithms or software that are central to the research but not yet described in published literature, software must be made available to editors/reviewers upon request. We strongly encourage code deposition in a community repository (e.g. GitHub). See the Nature Research guidelines for submitting code & software for further information.

Data

Policy information about availability of data

All manuscripts must include a data availability statement. This statement should provide the following information, where applicable:

- Accession codes, unique identifiers, or web links for publicly available datasets
- A list of figures that have associated raw data
- A description of any restrictions on data availability

Supplementary Table 6 contains raw data from Figs 1-7 and Supplementary Figs 2-6. The datasets generated during and/or analysed during the current study are available from the corresponding author upon reasonable request. Mass spectrometry data have been deposited in ProteomeXchange with the primary accession code is PXD 010460.

Field-specific reporting

Please select the best fit for your research. If you are not sure, read the appropriate sections before making your selection.

☒ Life sciences ☐ Behavioural & social sciences ☐ Ecological, evolutionary & environmental sciences

For a reference copy of the document with all sections, see nature.com/authors/policies/ReportingSummary-flat.pdf

Life sciences study design

All studies must disclose on these points even when the disclosure is negative.

Sample size	For cell migration studies or chemotaxis assays, sample sizes were chosen according to how many cells could reliably be tracked in the assay. For manual tracking, we tracked at least 30 cells per experiment with 3 independent repeats. In some cases, where automated tracking was used, sample sizes were larger e.g. in Figure 6j-n and Supplementary Figure 5g-h, more than 500 cells were tracked. The sample size was not pre-chosen, but was kept constant within an experiment and was based on the maximum number of cells that could be reliably analysed within a reasonable time frame.
Data exclusions	We did not exclude any data points.
Replication	All experiments were reproduced at least 3 times independently, except for 1) the SPR, which has been done once, in a forward and reverse way. 2) PLA experiment from Supplementary Figure 2k, only done twice, and WB for parental WM852 cell line only done twice. All attempts at replication were successful and all experiments can be reproduced.
Randomization	We did not randomise our experiments, but independent cultures or passages were used for each independent repeat and done on different days.
Blinding	Our studies were not done blind, but we used computer-based tracking and analysis with as many cells as was practical to track/analyse to minimise bias.

Reporting for specific materials, systems and methods

Materials & experimental systems

n/a	Involved in the study
☐	☒ Unique biological materials
☐	☒ Antibodies
☐	☒ Eukaryotic cell lines
☒	☐ Palaeontology
☒	☐ Animals and other organisms
☒	☐ Human research participants

Methods

n/a	Involved in the study
☒	☐ ChIP-seq
☒	☐ Flow cytometry
☒	☐ MRI-based neuroimaging

Unique biological materials

Policy information about availability of materials

Obtaining unique materials	All unique materials generated and described in this study will be provided upon reasonable request to the corresponding authors. Please request Dictyostelium reagents from Robert Insall and mammalian reagents from Laura Machesky.

Antibodies

Antibodies used

1) CYRI-B (Fam49B)- supplied by Sigma, cat. No HPA009076
2) CYRI-B (Fam49B)- supplied by Protein Tech, cat. No 20127-1-AP
3) D. discoideum CYRI- homemade (Biogenes)
4) GFP- supplied by abcam, cat No ab290
5) GST- supplied by abcam, cat No ab18183, clone GST.B6
6) Rac1- supplied by Millipore, cat No 05-389, clone 23A8
7) Alpha-tubulin- supplied by Sigma, cat No T9026, clone DM1A
8) CYFIP1- supplied by abcam, cat No ab154045
9) NCKAP1- supplied by abcam, cat No ab126061
10) WAVE2- supplied by Santa Cruz, cat No SC33549, clone H-110
11) Anti Rabbit 800nm- supplied by Thermo Scientific, cat No SA5-35571
12) Anti-Mouse 800nm- supplied by Thermo Scientific, cat No SA5-3552
13) Anti-Rabbit 680nm- supplied by Invitrogen, cat No A21206
14) Anti-mouse 680nm- supplied by Invitrogen, cat No A10038
15) HA-tag- supplied by Covance, cat No 901501, clone 16B12
16) MYC-tag- supplied by CST, cat No 2278, clone 71D10
17) Podocalyxin- made by David Bryant
18) Flag-tag- supplied by Sigma, cat No F1804, clone M2
19) Tubulin- supplied by abcam, cat No ab6160YL1/2
20) Cortactin- supplied by Millipore, cat No 05-180
21) P34-Arc- supplied by Millipore, cat No 07-227
22) Anti-Rabbit 488nm- supplied by Invitrogen, cat No A11008
23) Anti-Mouse 488nm- supplied by Invitrogen, cat No A11001
24) Anti-Chicken 488nm- supplied by Invitrogen, cat No A11039
25) Anti-Rat568nm- supplied by Invitrogen, cat No A11077
26) Anti-Rabbit 594nm- supplied by Invitrogen, cat No A21207
27) Anti-Mouse 594- supplied by Invitrogen, cat No A31203
See also Supplementary Table 3

Validation

1) CYRI-B (Fam49B)- supplied by Sigma, cat. No HPA009076- validated by Sigma for Western blot and additionally using control and knockout cells, this study
2) CYRI-B (Fam49B)- supplied by Protein Tech, cat. No 20127-1-AP- validated by Proteintech for Western blot and additionally using control and knockout cells in this study
3) D. discoideum CYRI- homemade (Biogenes)- validated by western blot using control and knockout cells, this study
4) GFP- supplied by abcam, cat No ab290 – validated by abcam for Western blot and immunofluorescence
5) GST- supplied by abcam, cat No ab18183, clone GST.B6 – validated by abcam for Western blot
6) Rac1- supplied by Millipore, cat No 05-389, clone 23A8
7) Alpha-tubulin- supplied by Sigma, cat No T9026, clone DM1A
8) CYFIP1- supplied by abcam, cat No ab154045 – validated by abcam for Western blot
9) NCKAP1- supplied by abcam, cat No ab126061 – validated by abcam for Western blot
10) WAVE2- supplied by Santa Cruz, cat No SC33549, clone H-110 -
11) HA-tag- supplied by Covance, cat No 901501, clone 16B12
12) MYC-tag- supplied by Cell Signaling Technology, cat No 2278, clone 71D10 -validated by CST for Western blot and immunofluorescence
13) Podocalyxin- made by David Bryant validated in 1: Bryant DM, Roignot J, Datta A, Overeem AW, Kim M, Yu W, Peng X, Eastburn DJ,Ewald AJ, Werb Z, Mostov KE. A molecular switch for the orientation of epithelial cell polarization. Dev Cell. 2014 Oct 27;31(2):171-87. doi:10.1016/j.devcel.2014.08.027. Epub 2014 Oct 9. PubMed PMID: 25307480; PubMed Central PMCID: PMC4248238.
14) Flag-tag- supplied by Sigma, cat No F1804, clone M2 – validated by Sigma for Western blot and immunofluorescence
15) Tubulin- supplied by abcam, cat No ab6160, clone YL1/2 – validated by abcam for western blot and immunofluorescence
16) Cortactin- supplied by Millipore, cat No 05-180 – validated by Millipore for Western Blot and immunofluorescence
17) P34-Arc- supplied by Millipore, cat No 07-227 – validated by Millipore for Western blot and immunofluorescence
See also Supplementary Table 3

Eukaryotic cell lines

Policy information about cell lines

Cell line source(s)

Cell line source: COS-7 were obtained from Cancer Research UK Cell Service, CHL-1 were obtained from ATCC, WM852 were from Prof. Dorothy Bennett (St George's University of London), HEK293T cells were obtained from Prof. Kevin Ryan (Beatson Institute for Cancer research), and MDCK were obtained from Prof. Keith Mostov (UCSF). MEF and mouse tail fibroblasts were generated in our laboratory.

Authentication

Cell lines were not independently authenticated

Mycoplasma contamination

Cell lines were routinely tested for mycoplasma and were certified to be negative

Commonly misidentified lines
(See ICLAC register)

Commonly misidentified lines: No cell lines used in this study were found in the database of commonly misidentified cell lines that is maintained by ICLAC and NCB BioSample.